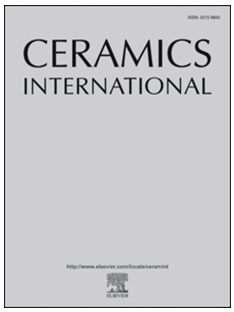

A novel synthesis from instability difference between SiC 3-C and 6-H crystal to form nanoparticles stems by alkali solution and its degrading various environmental pollutants

Zhiqi Zhu, Santosh K. Tiwari, Yu Chen, Daohan Liu, Shiming Yang, Kunyapat Thummavichai, Guiping Ma, Nannan Wang, Yanqiu Zhu

PII: S0272-8842(24)00631-X

DOI: https://doi.org/10.1016/j.ceramint.2024.02.135

Reference: CERI 39903

To appear in: *Ceramics International*

Received Date: 6 November 2023

Revised Date: 12 February 2024

Accepted Date: 12 February 2024

Please cite this article as: Z. Zhu, S.K. Tiwari, Y. Chen, D. Liu, S. Yang, K. Thummavichai, G. Ma, N. Wang, Y. Zhu, A novel synthesis from instability difference between SiC 3-C and 6-H crystal to form nanoparticles stems by alkali solution and its degrading various environmental pollutants, *Ceramics International* (2024), doi: https://doi.org/10.1016/j.ceramint.2024.02.135.

A Novel Synthesis from Instability Difference Between SiC 3-C and 6-H Crystal to Form Nanoparticles Stems by Alkali Solution and Its Degrading Various Environmental Pollutants

Zhiqi Zhu[1,2], Santosh K. Tiwari[1,3], Yu Chen[1,2], Daohan Liu[1], Shiming Yang[1], Kunyapat Thummavichai[2,4], Guiping Ma[5]*, Nannan Wang[1]*, Yanqiu Zhu[1,2]

[1] State Key Laboratory of Featured Metal Materials and Life-cycle Safety for Composite Structures, School of Resources, Environment and Materials, Guangxi University, Nanning 530004, Guangxi, China

[2] College of Engineering, Mathematics and Physical Sciences, University of Exeter, Exeter, EX4 4QF, United Kingdom

[3] Department of Chemistry, NMAM Institute of Technology, Nitte (Deemed to be University), Nitte 547110, India

[4] Department of Mathematics, Physics and Electrical Engineering, Faculty of Engineering and Environment, Northumbria University, Newcastle-upon-Tyne NE1 8ST, United Kingdom

[5] State Key Laboratory of Chemical Resource Engineering, Beijing University of Chemical Technology, Beijing 100029, China

* *Corresponding author: Guiping Ma, Nannan Wang*

E-mail: magp@buct.edu.cn, wangnannan@gxu.edu.cn

ABSTRACT

In this paper, the nano silicon carbide with different sizes was prepared without hydrofluoric acid by using simple milling and related low temperature etching process in normal pressure. Also, it was the first time verified that 3-C dominated crystalline form of polycrystalline silicon carbide is etched, leaving the 6-H silicon carbide crystalline form by the Raman spectra and HAADF-STEM (high-angle-annular dark-field scanning transmission electron microscopy) imaging that. The application of the alkali etching technique could precise control the partial structural transformation of silicon carbide crystals to a certain extent, which further expands the traditional crystal structure transformation process. In addition, this paper demonstrates the silicon carbide composites in photocatalytic removal of various organic pollutants from aqueous solutions. In the photo degradation of MB (Methylene Blue), the removal rate of the modified silicon carbide shown ten times as much as the commercial silicon carbide. The one-hour degradation efficiency was significantly higher in the 50 μL H_2O_2 system (100.0%, 86.8% and 89.9% removal of MB, Rhodamine B, Methyl Orange and Tetracycline hydrochloride, respectively). Furthermore, the unit spin concentrations of vacancy defects, superoxide radicals and hydroxyl radicals were quantitatively analysed. The vacancy defects of the etched material were 1000 times higher than before, and the modified silicon carbide had higher transmittance to infrared and visible light. It strongly absorbs ultraviolet light. Conversely, the research on micron-sized silicon carbide loaded with Ag and Pt atoms found that it had a nitrogen fixation effect during the warming up process, in a nitrogen atmosphere.

KEYWORDS: Nano Silicon-Carbide, Alkali Etching, Photocatalysis, 0-D Nanostructures, Degradation

1 Introduction

The large-scale use of organic polymer dyes, medical wastewater and environmental hormones (e.g. pesticides) has led to a serious crisis of water pollution. The severe contamination of water from various organic pollutants poses significant threats to human wellbeing. Effective measures are urgently required to solve the water pollution. Among wastewater pollutant treatment technology, composite catalyst is one of the efficient methods to degrade organic pollutants in water. The third-generation semiconductor material, also known as compound semiconductor material, is a type of material used in the manufacturing of electronic devices. It includes materials such as gallium arsenide, indium phosphide, and silicon carbide. These materials offer superior performance compared to their first and second generation counterparts, making them highly sought after in the electronics industry. They are particularly known for their high electron mobility, high temperature resistance, and high frequency response[1]. Silicon carbide (SiC), is considered as an ideal candidate catalyst support material and reaction interface material of photocatalytic reaction, due to its excellent characteristics like wear resistance, corrosion resistance, broadband system, and stable physical and chemical properties[2]. Researches have been conducted to study the photocatalytic properties of SiC; however two main challenges, including high production cost and low specific surface area, remain and limit further development of SiC.. The current mainstream synthesis paths of SiC include sol gel method, laser induced vapor phase reaction synthesis[3], thermochemical vapor phase reaction method and hydrofluoric acid etching. The cost of the above preparation method is relatively high. Thus, finding ways to increase the specific surface area of silicon carbide has been one of the hotspots in SiC research. Therefore, comparing the mechanism of SiC preparation[4-7], we propose a new way to oxidize silicon carbide by alkali etching with a low cost.

Nanosized silicon carbide has fascinating charm due to its defects in the field of optoelectronics. Pecific defects in SiC exhibit electronic states that display pronounced optical and spin transitions. As a foundational base for quantum information processing and nanoscale detection operations, they are progressively gaining recognition[8-10]. The

77 modifications and the exploration of various properties in the field of silicon carbide
78 nano-surfaces are diverse. Commercial SiC powders with a size greater than 100 nm
79 were subjected to etching using nitric acid and hydrofluoric acid.

80 At a molecular level, Peng et al.[11-12] examined how the hydrophilic properties of
81 SiC QDs were affected by surface hydroxyl groups during CO_2 hydrogenation. Zhu et
82 al.[13] used pulsed laser ablation to fabricate SiC QDs from a hexagonal silicon carbide
83 polycrystalline target submerged in ultrapure water. The production and luminescent
84 properties of SiC QDs, originating from distinct polytypes of bulk SiC crystals, were
85 reported by Fan et al.[14-16], using an electrochemical method. Li et al.[17] synthesized
86 highly ordered SiC crystal whiskers with a large aspect ratio by carbothermal reduction
87 of silica using carbonized organic polymers (resins) as mixed precursors. A method of
88 magnesiothermic reduction synthesis has also been reported, which can convert two
89 different nanomaterials, SiO_2/C, into SiC materials, maintaining their crystalline
90 organizational structure even at temperatures as low as 600 degrees Celsius[18]. Finally,
91 Luo et al. fabricated a nanoscale silicon carbide coating on the graphite surface using
92 laser irradiation and investigated the impact of variations in laser energy density on the
93 coating[19-20]. Certain reports have studied thermodynamic calculation and various acid
94 to spatially define the etching morphology[21-22]. Cambaz et al.[23] have shown a technique
95 to create nanometer size or intricate, well-structured novel material from SiC. Their
96 study revealed that selective removal of 3C-SiC can be achieved by etching SiC
97 whiskers with a mixture of two strong acids (nitric acid and hydrofluoric acid) at 100 ℃.
98 This leads to the creation of elaborate pagoda-like crystal structures. Khuat and
99 colleagues presented a straightforward technique for creating through holes in 6H-
100 SiC[24-26]. This method combined femtosecond laser exposure and selective chemical
101 etching using a blend of HF and HNO_3. Their findings indicated that the surrounding
102 areas of the holes maintained their original chemical compositions of silicon and carbon.
103 Zhang et al.[27] employed molten KOH to refine SiC, with the pace of the process being
104 strongly linked to the temperature. This led to an extremely rapid polishing of lamellar
105 SiC, decreasing the roughness from submicron to nanoscale in a very short period of
106 time (minutes), at 800 ℃.

Herein, we successfully prepared micron SiC, 50-100 nm SiC and SiC QDs. Based on many kinds of composite electrode materials containing silicon carbide, they all had extremely stable cycle characteristics and corrosion resistance under proton solution or weak acid conditions[28-30]. It was the first time discovered that the 6-H crystalline form is more stable than the 3-C crystalline form under relatively high concentration of alkali solution. Finally the etched SiC's application in the photocatalytic degradation of MB, Rhb and TCH at the trace hydrogen peroxide (50 μL) reached 98.6%, 86.8% and 89.9%, respectively. The concentration of various free radicals on the material surface was quantitatively analysed.

2 Experimental

2.1 Chemical Reagents

Green silicon carbide (polycrystalline)(SiC), sodium hydroxide (granular, analytically pure)(NaOH), ethanol (99%)(C_2H_5OH), potassium chloroplatinate (K_2PtCl_6), silver nitrate ($AgNO_3$), Methylene Blue ($C_{16}H_{18}ClN_3S$), Rhodamine B ($C_{28}H_{31}ClN_2O_3$), Methyl Orange ($C_{14}H_{14}N_3SO_3Na$), Tetracycline hydrochloride ($C_{22}H_{25}ClN_2O_8$), 2,4-Dichlorophenol ($C_6H_4Cl_2O$), Atrazine ($C_8H_{14}ClN_5$) and other conventional reagents are commercially sourced. Analytical-grade chemicals obtained from Shanghai Chemical. The water used in this experiment is ultrapure water, and the water for washing experimental apparatus is deionized water.

2.2 Preparation of Nano SiC

Commercially purchased silicon carbide was placed in a vertical planetary mill, and ground at a speed of 400 rpm for 6 hours. Then it was passed through a 400-mesh sieve to obtain fine silicon carbide powders. In the procedure, 10 grams of SiC powders and 20 grams of sodium hydroxide in granular form were dissolved in 120-150 mL of deionized H_2O. The resulting solution was then heated to boiling for 2 hours and stirred at 400 rpm in a water bath (chosen based on preliminary experiments to balance etch rate and control over the phase composition of the silicon carbide.). Post cooling to

ambient temperature, the coarse SiC was gathered by performing centrifugation at 2000 rpm for a 10-minute duration. Subsequently, the supernatant was centrifuged at 4000 rpm, yielding a micron SiC precipitate. The remaining supernatant was centrifuged again at 10000 rpm, resulting in nano SiC sediment. SiC products of varying sizes obtained from each stage of centrifugation were thoroughly washed with fluid mixture (Up water and ethanol). At last, the moist, washed samples were dried at a temperature of 60 ℃ for a 6-hour span (optimized for effective moisture removal without damaging the sensitive nanostructures). The principle of the liquid phase-based reaction could be illustrated as shown in Equation (1). The oxygen in the reaction process is derived from air.

$$O_2 + SiC + 2NaOH + H_2O \longrightarrow Na_2SiO_3 + CO_2 \quad (1)$$

2.3 Preparation of SiC QDs solutions

The nano-sized SiC powders were dispersed in 20 mL of ultrapure water and ultrasonically processed for a full hour. The solution was then spun at a speed of 8000 rpm for 7 minutes, followed by ultracentrifugation of the remaining supernatant at 12000 rpm for 15 minutes. The resulting wet powder was allowed to dry at a temperature of 60 ℃ for a 12-hour period. This process resulted in the acquisition of SiC Quantum Dots (QDs) having an average particle dimension between 5 and 10 nanometers.

2.4 Loading precious metal experiment: metal@etched micron SiC

The obtained micron silicon carbide (0.1 g) was mixed with commercial K_2PtCl_6 (5% load) and silver nitrate (5% load), respectively, and heated to 60 ℃ for 10 hours in a 1:1 mixed solution of ethanol and water (10ml in total). The substance was first spun at 8000 rpm for a duration of 10 minutes in a centrifuge. Following this, it underwent ultrasonic treatment for half an hour. It was then cleansed using deionized water before being dried in a 60 ℃ oven for a period of 12 hours, resulting in a dry powder.

2.5 Instrumentations

The catalyst's composition was analyzed using X-ray diffraction with Cu Kα radiation (XRD, Rigaku D/MAX 2500 V, Japan) at a scanning speed of 5° per minute, recording scans in the 2θ range of 5-85 degrees. The catalysts' surface morphology was inspected using field emission scanning electron microscopy (FESEM, Hitachi S-4800, Japan) and high-angle-annular dark-field scanning transmission electron microscopy (HAADF STEM). Absorbance spectra were analyzed with a UV-Vis Spectrophotometer (TU-1901, Persee) at room temperature. The samples' Brunauer-Emmett-Teller (BET) surface area and nitrogen adsorption isotherms were measured using a Micromeritics ASAP 2460 adsorption instrument. Photoelectrochemical tests were conducted on a Multi Autolab/M204 electrochemical station at room temperature. The Electron Paramagnetic Resonance Spectroscopy (EPR) test was conducted by Bruker EMX PLUS, Germany. When testing the vacancy defects, the quartz tubes were weighed and loaded according to the material serial number. Then the quartz tubes were placed in the center of sample cavity, using deionized water or methanol as solvent (different systems will be used for other projects) to prepare 1 mg/ml samples. After ultrasonic dispersion for 5 min, mix 30 μL sample and 30 μL DMPO (100 mM deionized water/methanol as solvent) evenly. A certain amount of mixed solution was taken with a capillary tube and covered by a quartz tube, which was placed into an EPR sample chamber to test vacancy defects, hydroxyl radical and superoxide radical. The PLS-SXE 300D xenon lamp light source, with a power of 300w and 15A, is produced by Beijing Porphyry Technology Co. The JEM-ARM200F model spherical differential electron microscope is another product.

The oxidation of MB was carried out in a glass reactor using 20 mg of raw SiC and etched nano SiC, dispersed in 100 mL solution (10 ppm MB). The suspensions were subjected to ultrasound for 10 minutes and stirred in the darkness for 30 minutes to reach adsorption equilibrium. The photocatalytic tests were then performed by irradiating the suspensions under vigorous stirring with a Xenon lamp (Perfect light PLS-SXE300) that emitted a full light spectrum at an intensity of 180 mW/cm^2. The

purpose of this experiment was to reduce the concentration of MB through photocatalytic oxidation using SiC as the catalyst. Every 10 minutes, 5 mL of the suspension was collected and centrifuged at 8000 rpm to minimize catalyst interference. The photocatalytic degradation efficiency of MB was then determined based on the absorbance. The catalytic properties of the nano silicon carbide produced were compared with commercial SiC in terms of degradation of MB, MO, Rhb, 2,4-DCP, ATZ, and Tetracycline hydrochloride.

3 Results

3.1 Characterizations

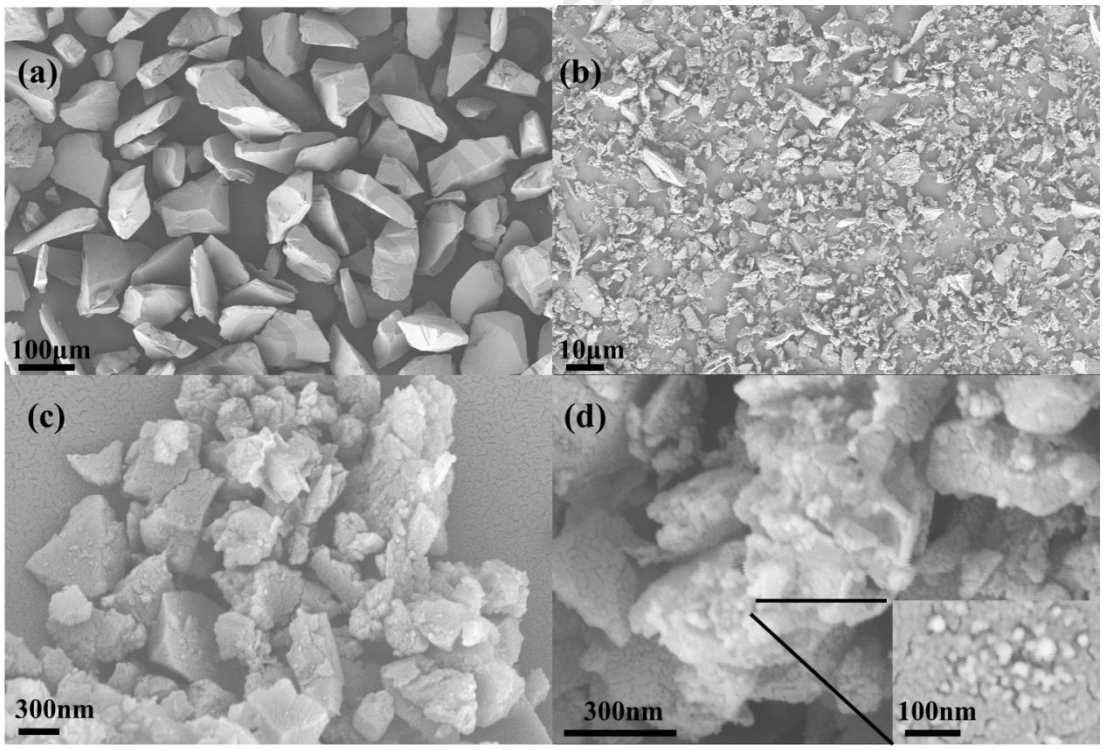

Figure 1 SEM images of (a) Commercial SiC, (b) Etched micron SiC, (c) Etched nano SiC, (d) SiC QDs agglomerated together on large blocks of SiC, respectively (inset: corresponding enlarged image).

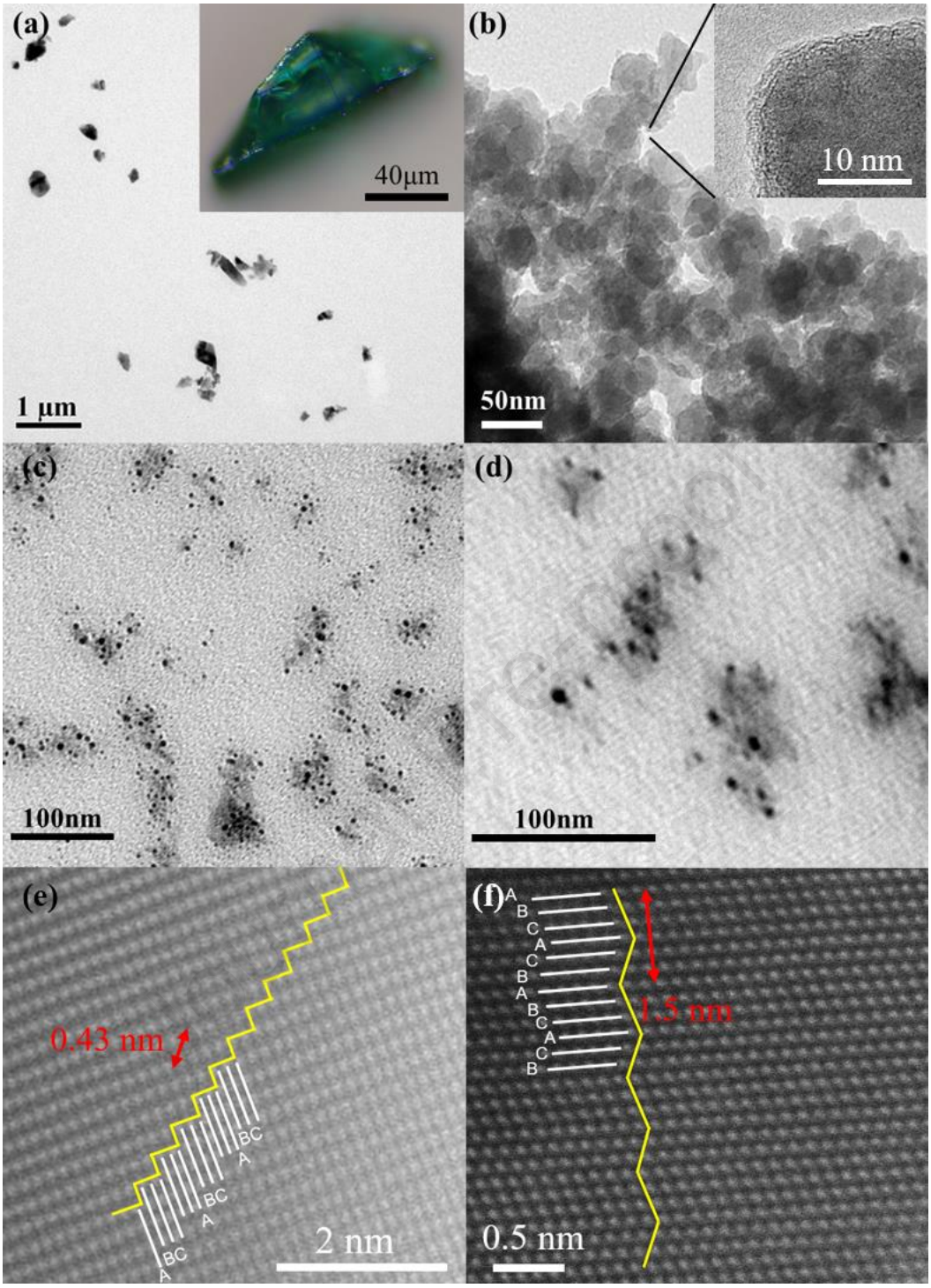

Figure 2 TEM images of (a) Ball milled micron SiC, (b) Etched nano SiC, (c) SiC QDs, and (d) Magnification of SiC QDs, respectively. （e）HAADF-STEM image of commercial 3-C SiC and (f) etched nano SiC sample. Schematic columns of atoms are overlaid on the HAADF-ST EM image where the yellow and white line represent the crystal types.

Fig. 1(a) presents the scanning electron microscope depiction of commercially available silicon carbide. Fig. 1(b-d) illustrate the transformation process of bulk silicon

carbide following ball milling and etching. These figures demonstrate that as particle size decreases, the nano silicon carbide after alkali etching has a larger specific surface area and a more uneven surface. Fig. 2(a) presents the TEM image of ball-milled micron SiC and the commercial SiC's color image under the digital microscope. Then, Fig. 2(b) indicates that the etched silicon carbide is sculptured into a nearly spherical shape with a diameter of about 50 nm. These particles tend to agglomerate and cement each other. This morphology is consistent with the products observed in the carbothermal reduction or sol-gel method, which had a rough surface. Much spherical nano SiC are loaded on micron-sized flake SiC. Fig. 2(c-d) reveal that the silicon carbide can be etched to prepare silicon carbide quantum dots. It was firstly observed by the HAADF STEM that the crystal form of nano SiC was etched by alkali solution. The crystalline forms of more than three particles were counted. In Fig.2 (e), the atomic stacking period length is 0.43 nm, conforming to 3-C crystal form: ABC. Fig. 2 (f) shows the etched nano silicon carbide with an atomic stacking cycle length was 1.5 nm, conforming to 6-H crystal form: ABCACB. Combined with the Raman contrast diagram, commercial silicon carbide contains a mixture of 3-C, 4-H and 6-H crystalline forms. SiC is unstable in an alkali environment. Therefore, 6-H silicon carbide has higher stability than 3-C silicon carbide when undergoing alkali etching, and still maintains a high degree of crystallinity. The mechanism confirms that the 3-C crystalline form has an approximate angle of 90 degrees. The atoms are arranged in a laminar pattern, which makes it easier for intercrystalline slip. In contrast, the 6-H crystalline form has a clamping angle nearly 120-160 degrees, and the array arrangement tends towards an equilateral triangle. Under warming and the action of hydroxide ions, this process selectively removes less stable phases, thereby enriching the 6-H phase due to its relative stability and resistance to the etching process. The aforementioned etching process is akin to a precise interface control technique. This directional etching process can preserve the more stable 6-H crystal form, which holds immense application value in enhancing the single-crystal silicon carbide of electronic devices.

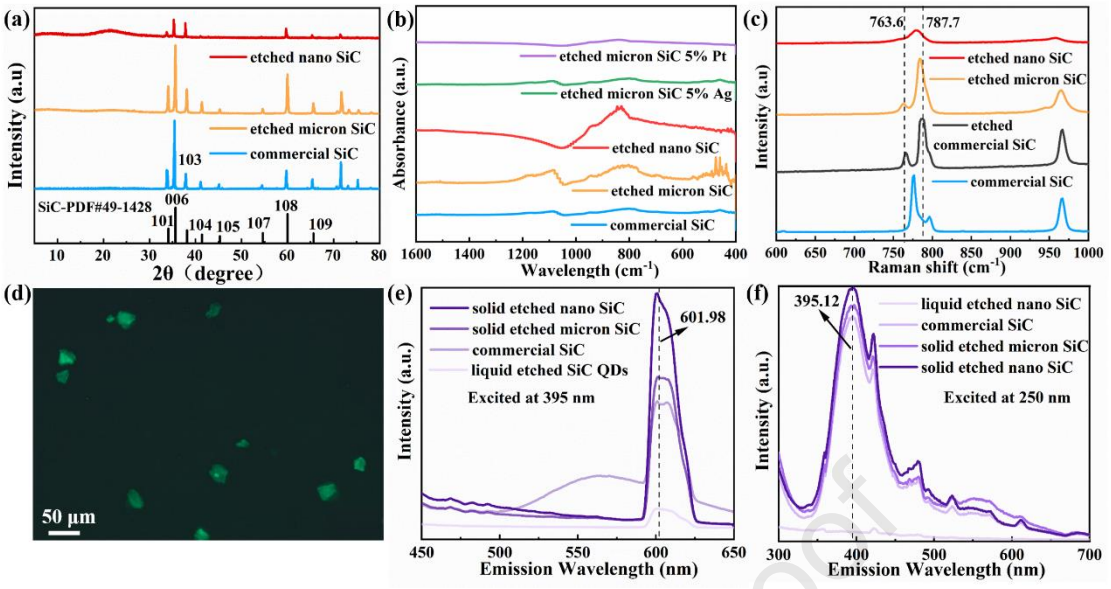

Figure 3 The as-produced samples, encompassing original SiC, etched micron SiC, and etched nano SiC, are featured in Figure 3. This includes (a) XRD, (b) FTIR, and (c) Raman patterns. The representation in (d) illustrates micron silicon carbide as visualized under a fluorescence microscope. Patterns of room-temperature photoluminescence in the acquired SiC samples are analyzed in panels (e) and (f). The purple lines lighten and darken to represent liquid etched nano SiC，commercial SiC，solid etched micron SiC and solid etched nano SiC

Fig. 3(a) shows XRD patterns of commercial SiC, etched micron SiC and etched nano SiC, respectively. There are eight distinct sharp peaks located at 34.1° ,35.6° , 38.1° , 41.3° , 45.3° , 54.6° , 59.9° , 65.6° . Based on the ICDD Data, JCPDS Card (No. 49-1428)[31], these diffraction peaks can be attributed to the diffraction of (1 0 1), (0 0 6), (1 0 3), (1 0 4), (1 0 5), (1 0 7), (1 0 8) and (1 0 9) planes of SiC, respectively[32]. This indicates that this type of silicon carbide is relatively pure[33]. Fig. 3(b) shows a new intense band, with a broad range, centered at 825 cm^{-1}. This was observed in the etched coarse SiC[32]. This characteristic in the spectrum signifies the main stretching motion of the silicon-carbon (Si-C) bond, representing the fundamental vibrational mode involving the stretching of these chemical bonds[34]. Etched micron SiC at 825 cm^{-1} has a higher peak and, by comparison[35], indicates that the particle size of silicon carbide might be smaller[36]. After loading silver and platinum, the corresponding peaks of silicon carbide disappear, which may be owing to the corresp

onding hydroxyl group (-OH) on the surface being replaced by silver and plati num. Fig. 3(c) indicates the Raman spectrum of semi insulating 3C-SiC taken at 25 degrees celsius with 532 nm excitation[37]. The peak position of commerci al 3-C crystalline conforms to the literature report. The reduction in etching pa rticle size results in the main peaks shifting to 787 nm and 763 nm, confirmin g the traits of the 6-H crystal form[38-39]. After polycrystalline silicon carbide etc hing, 3-C silicon carbide content decreases, while 6-H silicon carbide content i ncreases. In general, with the decrease in particle size, the strength of correspo nding peaks of mixed crystalline silicon carbide powder becomes lower[37]. Fig. 3(d) demonstrates that micron silicon carbide emits green light under the fluore scence microscope. The excitation intensity was kept constant for all samples when comparing the photoluminescence spectra of different types. The slit widt h of excitation and reception was consistent. The parameters of the fluorescenc e microscope and the photoluminescence instrument are different. The different excitation wavelengths are used to show that the excitation intensity of the etc hed nano SiC is higher than the commercial SiC. Fig. 3(e) depicts the PL spe ctrum of commercial SiC, etched micron SiC and etched nano SiC recorded at room temperature, which selected an excitation wavelength of 250 nm[40]. The b road spectral band extends from 350 to 700 nm, with the highest peak approxi mately centered at about 395.12 nm. The PL spectrum is influenced by the siz e of the particles, and nearly all of them emit strong visible light at the same peak location. As shown in Fig. 3(f), under the excitation light intensity of 39 5 nm, the luminous intensity increased significantly with the decrease in particl e size[41]. However, compared with solid powder, the concentration of SiC quant um dots solution was inferior, resulting in weak luminescence. According to pr evious literature studies, the morphology[42], location, and number of defects on the SiC surface have a significant influence on the luminescence intensity and peak position[43]. The peak emission at 395 nm is associated with near-band-edg e emission of SiC and a restrained quantum confinement effect. When electron s absorb corresponding energy and transit from the conduction band to the val

ence band, they recombine with holes, and generate photons and phonons simu ltaneously[44]. As an indirect semiconductor, 3-C SiC's photon energy (hν) is a c ombination of the band gap energy and the phonon energy (hν=Eg+Ep, where Ep represents the phonon energy) [45]. The optimal photoluminescence can be se en in etched SiC, thanks to the significant quantum confinement impact and th e quasi-direct band gap[46]. Hence, the energy of the photon surpasses the band gap of etched nano 3-C SiC, causing electron transition and producing more in tense yellow (600 nm) and purple light (400 nm). As discovered from Fig. S6-7, even under the condition of no light excitation and after the sedimentation of more than two weeks, obvious blue-violet light can be observed in the SiC QDs solution, indicating that SiC was etched to a sufficiently small nano size and uniformly distributed in the glass bottle[47].

3.2 Catalytic Performance in Degradation of MB, MO, Rhb, 2,4-DCP, ATZ, and Tetracycline hydrochloride

The adsorption-desorption isotherms (N_2) indicated the BET surface areas of etched coarse SiC, micron SiC, and nano SiC to be 1.0435 m^2/g, 3.3180 m^2/g and 8.5176 m^2/g, respectively, as shown in T1. More detailed specific surface area data are at ST5. To ensure the constant weight of each catalytic test, we kept the amounts of catalyst at 20 mg. Each experiment was conducted in the same laboratory, at the same ambient temperature, keeping the initial mixed solution neutral and on the same experimental instrument.

Table1 The BET Surface Area of Commercial SiC, Etched micron SiC and Etched nano SiC

Sample	Commercial SiC	Etched micron SiC	Etched nano SiC
BET-Surface Area/$m^2 \cdot g^{-1}$	1.0435	3.3180	8.5176

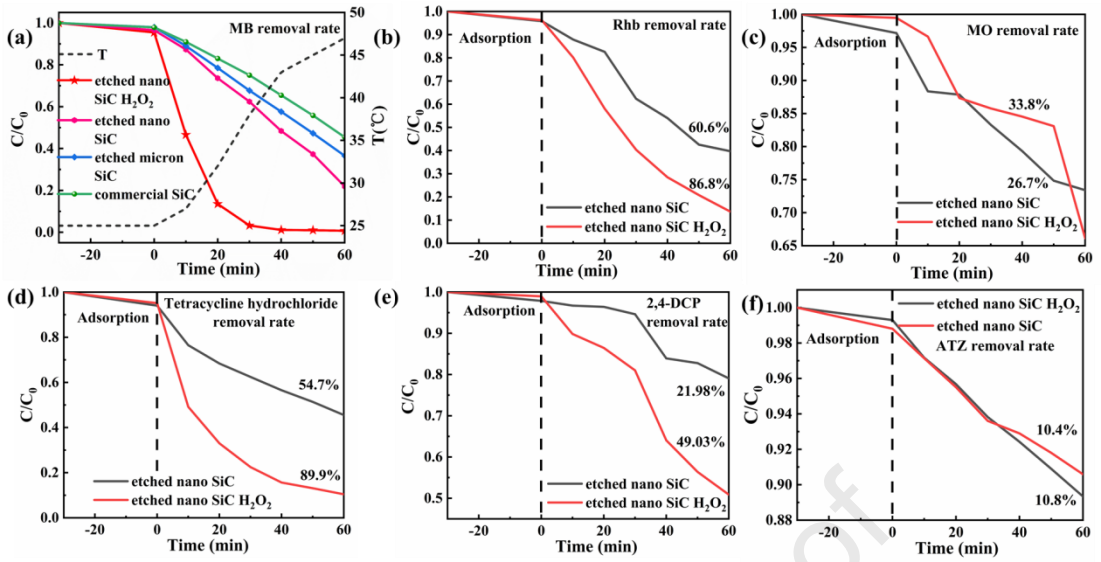

Figure 4 (a) The photocatalytic activity and temperature change of various silicon carbides to MB under the radiation of xenon lamp, and the photocatalytic activity of etched nano SiC to MB under 50 μL H_2O_2. (b-f); the study on the etched nano SiC's photocatalytic activity of RhB, MO, TCH, 2,4-DCP, and ATZ with or without the system of trace H_2O_2, respectively.

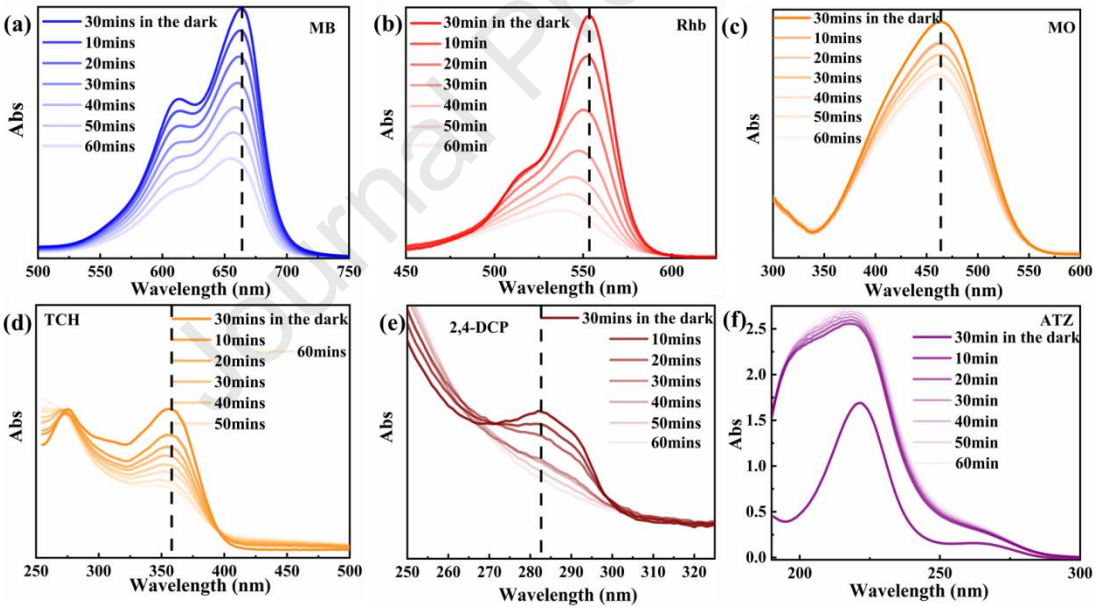

Figure 5(a-f); the trend chart of maximum ultraviolet absorption with the decrease of the concentration of MB, Rhb, MO, Tetracycline hydrochloride, 2,4-DCP, and ATZ, respectively. The lines deepen from light to dark, representing an increase in time.

As shown in Fig. 4 (a) compared with commercial silicon carbide and etched micro silicon carbide, etched nano SiC had a higher degradation rate. This may be based on its higher surface defect ratio. The etched nano SiC was used for the photodegradation of MB, RhB, MO, tetracycline hydrochloride, 2,4-DCP and ATZ. After 1 hour of full

spectrum irradiation, the degradation rates were 80.1 %, 60.6 %, 26.8 %, 54.7 %, 22.0 %, and 10.4 %, respectively. At trace hydrogen peroxide (50 μL), their efficiency reached 100.0 %, 86.8 %, 33.8 %, 89.9 %, 49.03 %, and 10.8 %, respectively. It was observed that the decomposition of H_2O_2 could provide oxygen radicals and synergize the decomposition of organic pollutants. In order to better evaluate the photo degradation of various organic substances by SiC, Fig. 5 shows the trend of maximum ultraviolet light absorption of various pollutants. During the breakdown process, the peak ultraviolet absorption of different organic materials exhibited a minor blue shift. This can be ascribed to the photochemical degradation of large organic molecules into smaller ones. The more detailed three-dimensional trend chart is shown in Fig. S8. To further corroborate the photocatalytic activity of different pH values and SiC under 50 μL H_2O_2 system, the photocatalytic activity of etched nano SiC with H_2O_2 at pH=3.08, 7.05 and 11.03 was analyzed under full spectrum xenon lamp irradiation in Fig. 6 (a) and (d), it was found that pH changed to 2.26, 6.10 and 8.67, respectively after 1 hour. In the system without H_2O_2, the corresponding pH decrease was also found after the reaction. This showed that a large amount of hydroxide ions was consumed in the silicon carbide photo-catalytic reaction system. In the system with a pH of 11 and trace hydrogen peroxide (50 μL), the photo degradation of MB of etched nano SiC reached 100% within 40 minutes. Additionally, the stability was further evaluated by conducting three consecutive cycles of the reaction using a 10 mg/L MB solution with 50 mg of etched nano SiC. After three cycles, over 99.7% of the initial activity remained in the degradation of MB, as depicted in Fig. 6 (b). This indicates the superior catalytic endurance of etched nano SiC and SiC/H_2O_2 on account of its stabilization in extreme circumstances. Consequently, etched nano SiC and etched nano SiC/H_2O_2 presented prominent activity and durability. Higher concentration MB solutions were used for the reaction. As depicted in Fig. S9, when the concentration of MB was elevated to 20 mg/L, the degradation efficiency over etched nano SiC under alkali conditions and etched nano SiC/H_2O_2 both reached 99% after 1 hour, respectively. The degradation kinetics of MB for all catalysts, as depicted in Fig. 6 (c and f), were subsequently examined. The kinetic constants of MB, MO, RHB, 2,4-DCP, ATZ and tetracycline hydrochloride

in trace H_2O_2 system were 8.869×10^{-2}, 5.420×10^{-3}, 3.31×10^{-2}, 1.153×10^{-2}, 5.86×10^{-3} and 3.578×10^{-2} min^{-1}, respectively. Fig. 6 (e) showed the degradation of MB by silicon carbide after etching under sunlight. Silicon carbide hardly degrades MB solution under sunlight, indicating that sunlight could not activate silicon carbide to generate photocatalytic activity. By comparison under the catalyst-free conditions (without SiC), the effective degradation efficiency of commercial SiC was less than 3%. However, the effective degradation efficiency of the etched nano SiC was 30%.

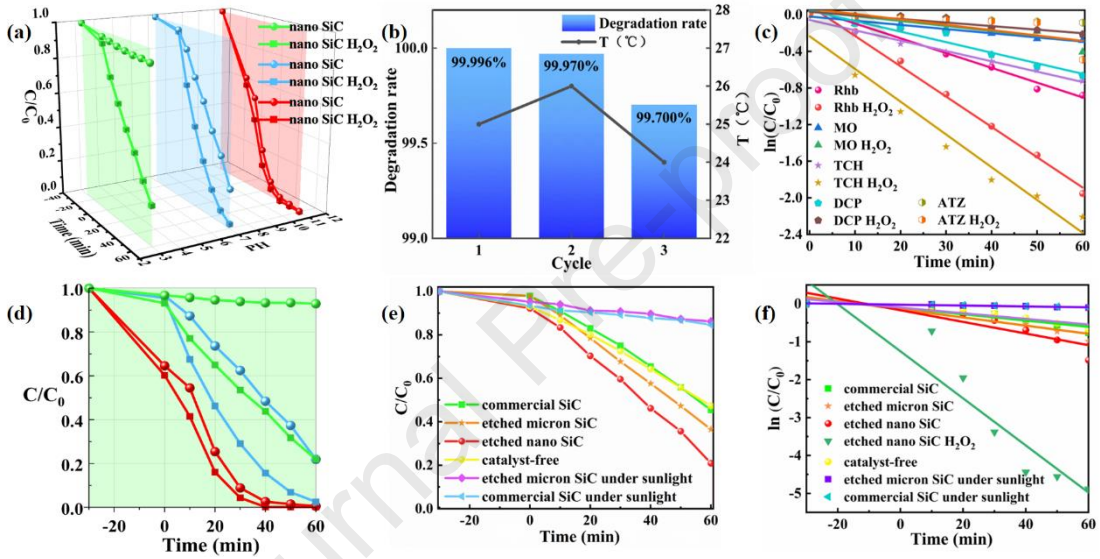

Figure 6 (a) the photodegradation performance of MB of etched nano SiC under different acid-base properties. (b); photocatalytic activity of etched nano SiC throughout three rounds of successive reaction. (c); Kinetic curves of MB, MO, RhB, 2,4-DCP, ATZ and tetracycline hydrochloride degradation. (d); the side overview of (a). The relevant detailed labelling has been shown in figure (a). (e); The photodegradation of 10 mg/L MB solutions with commercial SiC and etched nano SiC under sunlight. (f); Kinetic curves of MB under sunlight by commercial SiC and etched nano SiC.

3.3 Optical property and energy band structures

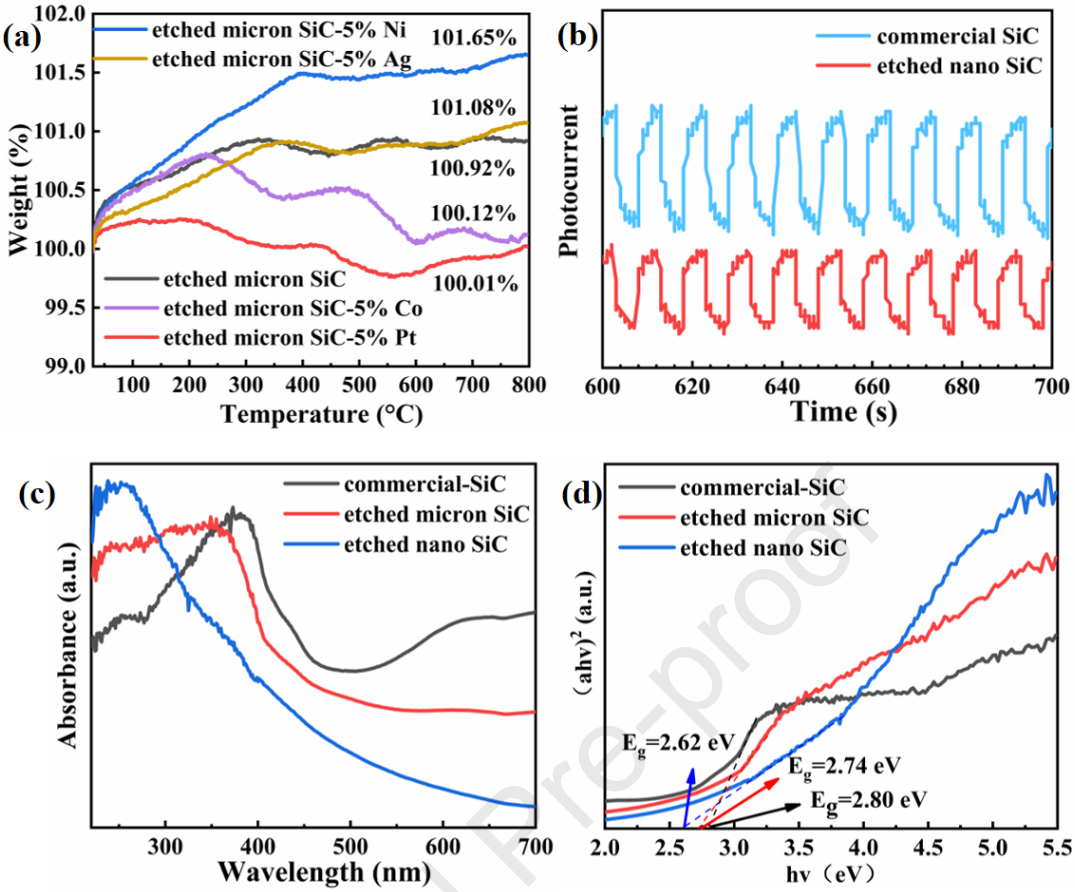

Figure 7(a) Thermogravimetric curve of the samples. (b) Photocurrent signals of commercial SiC and etched nano SiC under irradiation of Xenon lamp. (c) UV-vis spectra of the produced catalysts were obtained through diffuse reflectance. (d) The K-M function of commercial SiC and etched nano SiC was transformed for comparison.

Fig. 7 (a) presents a study on the Tg (Thermogravimetric) curve of etched micron SiC and various metal-loaded silicon carbides from 25-800 ℃ under a nitrogen atmosphere. It can be observed that the SiC loaded with Ag, Pt, Co, Ni had a certain amount of nitrogen adsorption, compared with etched silicon carbide. The weight percentage had increased significantly, especially the weight percentage of silicon carbide loaded with Ni and Ag had risen by 1.65% and 1.08%, respectively. Moreover, SiC was stable after etching at 800 ℃. Compared with other photocatalysts based on silicates of Fig. ST1, etched nano silicon carbide had superior advantages. As a bonus, silicon carbide can stabilize at high temperatures, which was more conducive to being a environmentally friendly photocatalyst. Silicon carbide doped with metal has a high application prospect in nitrogen adsorption at high temperatures in the future. First-principle calculations have shown that both Si- and C- surfaces, with Si and C as active

406 sites, can capture and activate dinitrogen. This mirrors the catalytic properties of
407 commonly used B-based electrocatalysts[48]. After careful analysis, Fig. 7(b) reveals that
408 the photocurrent signals generated by etched nano-scale silicon carbide (SiC) are
409 significantly lower than those from commercial SiC when exposed to irradiation from
410 a Xenon lamp. This reduction in photocurrent can potentially be attributed to the
411 formation of specific functional groups and free radicals on the nano SiC surface as a
412 result of the etching process. These surface modifications may hinder photon absorption
413 by introducing non-conductive paths or scattering centers, thereby reducing the
414 efficiency of photocurrent generation. According to Fig. 7 (c-d), the study of optical
415 properties was conducted to comprehend the mechanism of photocatalysis and the
416 process of charge transfer. To explicate the origin of the remarkable catalytic activity
417 for commercial SiC and etched nano SiC, the corresponding photocatalytic mechanism
418 was further explored. Furthermore, the catalyst's sensitivity to Xenon lamps light was
419 pivotal in enhancing the catalytic efficacy. As revealed by the UV-vis spectra of these
420 catalysts (Fig. 7 (c)), all procured SiC powders demonstrated robust absorption in the
421 ultraviolet area (< 400 nm). Nevertheless, the absorption of etched nano SiC in the
422 visible area (400 - 780 nm) was relatively less compared to commercial SiC and etched
423 micron SiC. In Fig. 7(d), the band gaps of etched nano SiC and etched micron SiC were
424 estimated to be 2.62 and 2.74 eV, respectively, using a reformed Kubelka-Munk (K-M)
425 function. Simultaneously, the band gap of commercial silicon carbide was assessed to
426 be 2.80 eV. The reduced band gap energy appeared sensitive to visible light in the
427 diffuse reflectance UV-vis spectra. When the semiconductor encountered light energy
428 surpassing its band gap, electrons were excited to the CB, thereby vacating holes in the
429 VB. The reaction of commercial SiC and etched micron SiC to irradiation was
430 additionally validated by the ephemeral photocurrent responses, which were gauged
431 using the photoelectrochemical approach. In fact, the quantum size effect results in an
432 expanded energy gap as the size of the particle diminishes, and concurrently, the gap
433 between the energy levels of the molecular orbitals occupied by the electrons decreases.
434 This leads to an increase in the energy levels of the unoccupied molecular orbitals,
435 which primarily accounts for the blue shift. Consequently, the curtailed recombination

of photogenerated carriers supports an enhanced use of electron-hole pairs for the production of oxidative radicals.[49]. Consequently, compared to its untreated counterpart, nano-scale silicon carbide (SiC) subjected to etching processes exhibits an enriched surface with free radicals, thereby significantly enhancing its sensitivity to photon stimulation within specific spectral regions emitted by xenon lamps, such as the ultraviolet to visible light range.

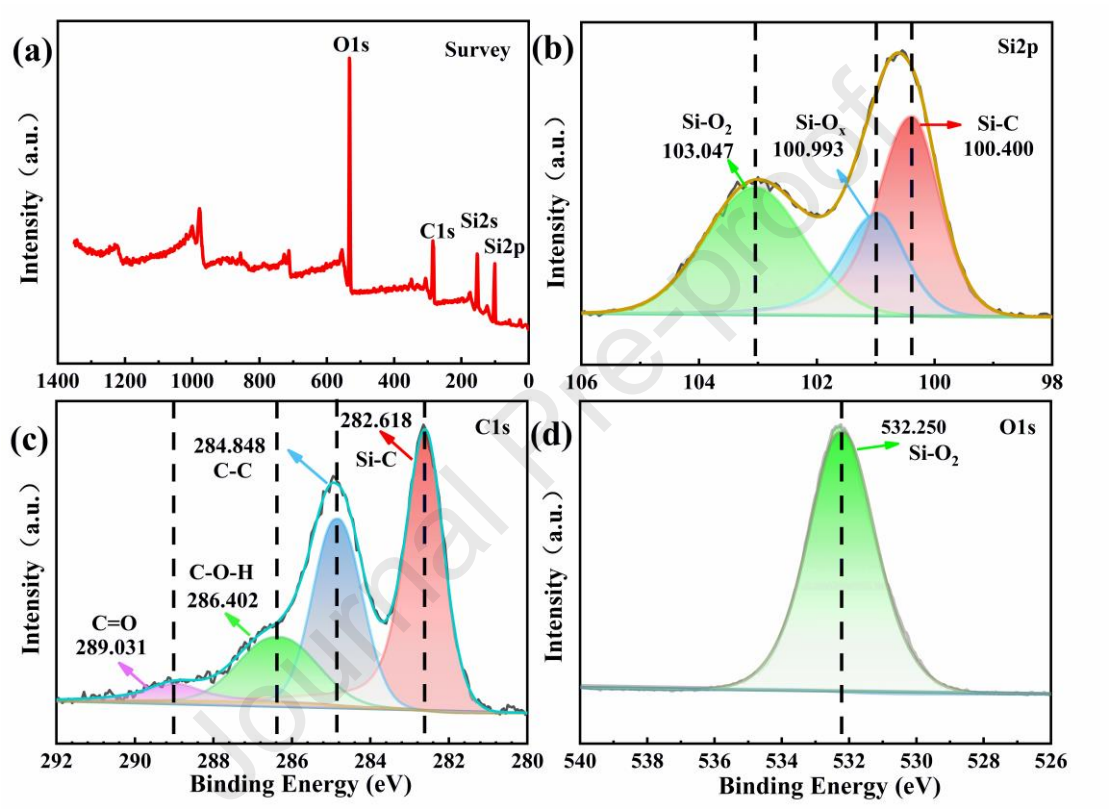

Figure 8 illustrates (a) the XPS survey spectra, (b) the Si 2p XPS spectra, (c) the C 1s XPS spectra, and (d) the O1s signals of commercially available SiC.

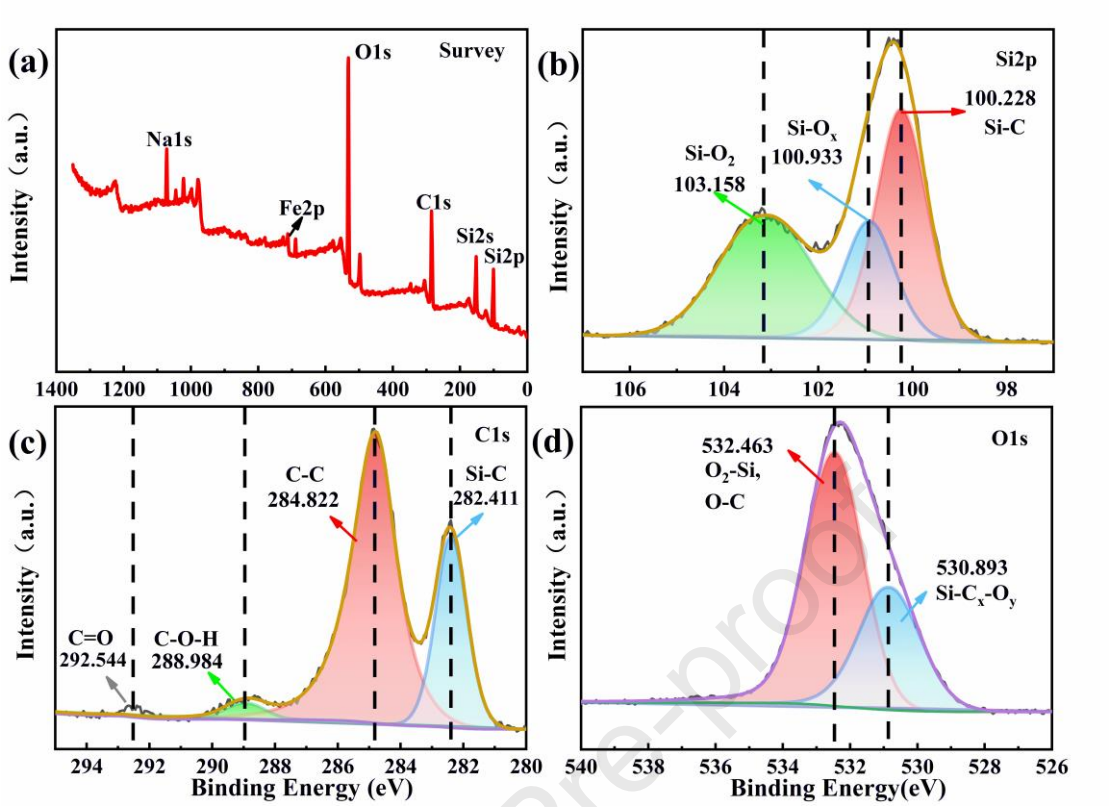

Figure 9 displays (a) a survey of XPS spectra, (b) XPS spectra for Si 2p, (c) XPS spectra for C 1s, and (d) O1s signals for etched nano SiC.

3.4 Mechanistic studies

The XPS wide scan spectra, Si 2p, C 1s, and O 1s energy loss spectra for both the commercially available SiC and the etched nano SiC are depicted in Fig. 8-9 (a), (b), (c), and (d) respectively. The calibration of all the XPS spectra and peaks was done using C 1s at 284.8 eV. The primary elements identified throughout the complete XPS spectra (Fig. 8 (a)) were Carbon (C), Silicon (Si), and Oxygen (O). The higher percentage of carbon than silicon may be attributed to the legacy of the carbon source during the preparation process. However, in Fig. 9, the peaks of Na1s and Fe2p were caused by alkali etching and impurities. As depicted, the photoelectron peaks at 532.25, 284.85, 150.98, and 100.55 eV can be attributed to O 1s, C 1s, Si 2s, and Si 2p, correspondingly.

The configuration of the Si 2p core level lines for the unaltered SiC surface and its transformation with the etching process are displayed in Fig. (8) and (9). The Si-C and Si-Ox peaks for the purified surface are situated at a BE of 100.4 eV and 100.9 eV,

respectively[50-51].Their peak shifts by 0.172 and 0.006 eV towards a lower BE respectively after etching[52]. The slight shift towards lower energy observed in the Si-Ox, Si-C and C-C bands of etched nano SiC, compared to commercial samples, indicates an increased electron transfer from C and O to Si, as well as a heightened interaction between C, O and Si. This blue shift may mean that the size of silicon carbide was reduced, and a large number of vacancies were generated on the surface[53]. The C 1s peak primarily consists of two elements, with the initial one linked to C-Si connections and the latter associated with C-C connections[54]. Furthermore, C-O-H and C=O peaks were decreased, and C-C and C-Si peak shifts by 0.026 and 0.207 eV towards a lower BE [55], which came from etching. The peak's shape resembles that acquired from previous experiments[56]. Considering that the shifts in Si 2p and C 1s were within the range of measurement precision, it confirms substantial electron transfer at the interface. This may be attributed to the appearance of the XPS peak (530.893 ev) of Si-C_x-O_y and the decrease of C=O and C-O-H peaks after etching. In the following EPR test (Fig. S7)[57], the concentration of various free radicals was calculated quantitatively to verify the photocatalytic performance.

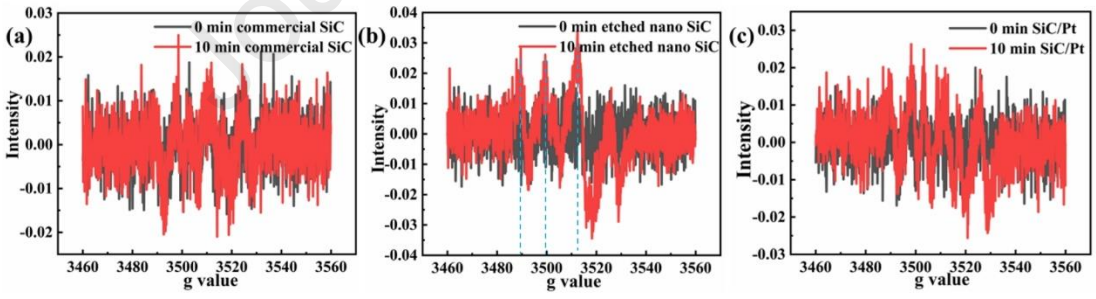

Figure.10 EPR superoxide radical signal of (a) commercial SiC, (b) etched nano SiC and (c) SiC-Pt with 0 min in the darkness and 10 mins under xenon lamp in the experimental data.

To quantitatively study the content of various free radicals, we carried out an experimental scheme. The experiment was initiated in complete darkness at 0 min and then conducted for 10 minutes under a xenon lamp. The content of free radicals was measured using a Bruker EMX PLUS instrument. This measurement helped verify the reason for the observed photocatalytic performance[58]. As shown in Fig. 10 (a-c), the

etched nano SiC in a dark environment did not exhibit any significant peak. However, under a xenon lamp for 10 minutes, a strong superoxide radical peak was observed. This was in contrast to commercial SiC and SiC-Pt, which demonstrated a certain contribution to the photocatalytic degradation of pollutants. Through the EPR experiment and the test of Fig. SEq.2 and 3, we quantitatively calculated the concentration of the superoxide radicals, as shown in Fig. S2. Fig. 10 (b) is the relatively representative and the better front type, indicating that the spin concentration per milliliter of etched nano SiC was 4.182×10^{12}.

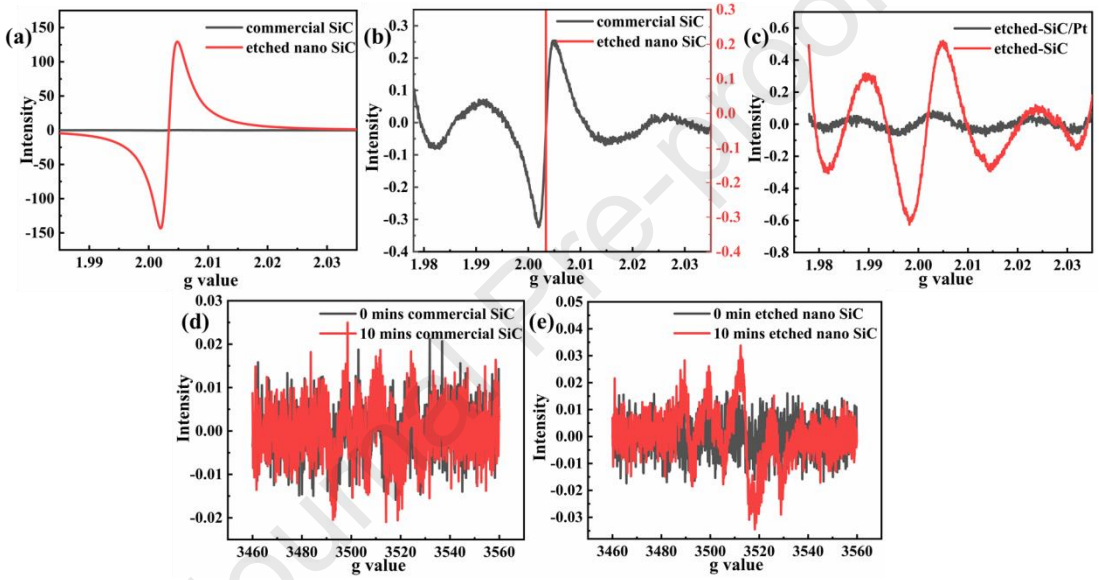

Figure 11 EPR vacancy defects signal of (a) commercial SiC and etched nano SiC. (b) the diagram shows the magnification of (a) at a g value of 2.004, (c) etched SiC and etched SiC-Pt with 0 min in the darkness and 10 mins under xenon lamp in the experimental data. (d) and (e) commercial SiC and etched nano SiC with 0 min in the darkness and 10 mins under xenon lamp in the experimental data.

As shown in Fig. 11 (a-b), it is evident to observe that the vacancy defects peak signal intensity of etched nano SiC is close to 150 (600 times that before the reaction). In contrast, the peak for commercial SiC was less than 0.25. As the size of the particle decreases and the specific surface area increases, the impact of alkali etching becomes more apparent[59]. This leads to a significant increase in surface vacancies and defects. The signals in Fig. 11 (d) and (e) indicates that no new vacancy defects were produced in the unetched commercial SiC under dark or light conditions. Under xenon light, the

vacancy defects of the etched nano SiC showed a corresponding weak peak, which indicates that vacancy defects are sensitive to light and play a dominant role in photocatalytic contribution. Fig. 11 (c) suggests that the vacancy defects on the surface of SiC loaded with Pt will be occupied, hence reducing the photocatalytic activity. Fig. S3 quantitatively shows that the spin concentration of etched nano SiC is at 6.434×1015 spins/mm^3, while commercial SiC is at 7.646×1012 spins/mm^3. This shows that the gap between them has almost reached three orders of magnitude.

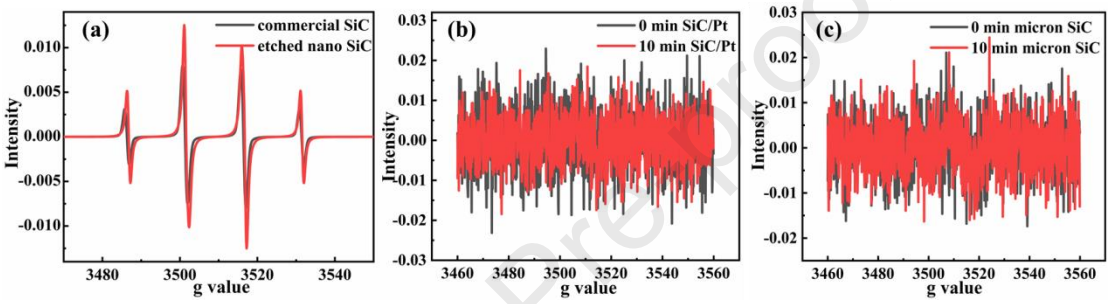

Figure 12 EPR hydroxyl signal of (a) commercial SiC and etched nano SiC, (b) SiC-Pt with 0 min in the darkness and 10 mins under xenon lamp in the experimental data. (c) etched micron SiC with 0 min in the darkness and 10 mins under xenon lamp in the experimental data.

Fig. 12 (a) also confirmed that the hydroxyl peak intensity of etched nano SiC is significantly higher than that of commercial silicon carbide after etching, which may be due to the relatively stable hydroxyl group formed on the surface after etching by sodium hydroxide. After repeated washing with alcohol and water, then centrifugal drying for 3h, it can also adhere to the surface of silicon carbide stably. Fig. 12 (b) shows there was no hydroxyl peak signal on platinum-supported SiC, which may be related to the defect position occupied by the platinum atom. Fig. 12 (C) demonstrated that there is no sign of a hydroxyl peak on etched micron silicon carbide, which may be caused by the particle size being too large, and the surface integrity of silicon carbide crystal was high, hence making it difficult for hydroxyl groups to attach . As shown in Fig. S4, the unit spin concentration of etched nano SiC was twice than the commercial SiC.

3.5 Photocatalytic mechanism

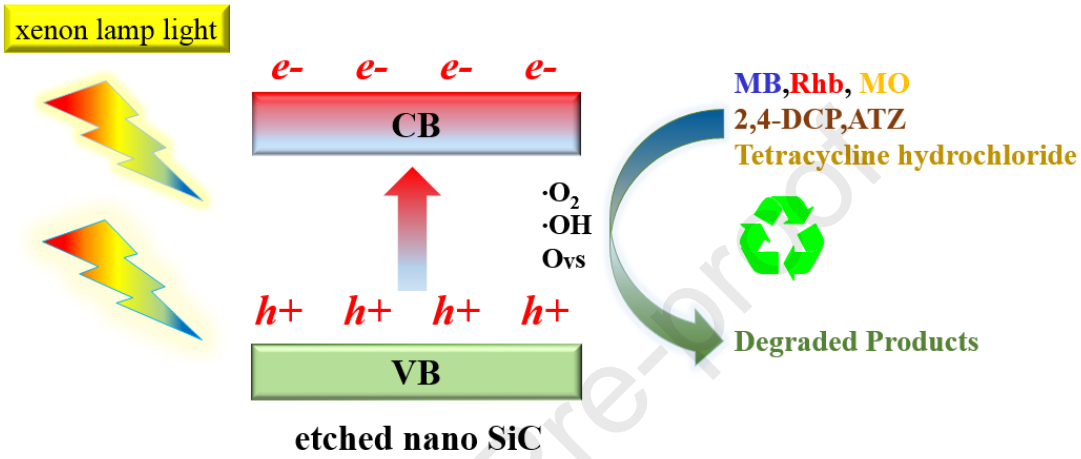

Fig. 13 Illustrations of the proposed photocatalytic mechanism over etched nano SiC .

$$SiC + h\nu \cdot \rightarrow \cdot h^{+} + e^{-} \quad \text{(Eq.4)}$$

$$h^{+} + H_2O \rightarrow OH^{\circ} + H^{+} \quad \text{(Eq.5)}$$

$$e^{-} + O_2 \rightarrow \cdot O_2^{-\circ} \quad \text{(Eq.6)}$$

Photocatalysis operates on the use of a photocatalyst, typically SiC, which is activated by UV-light to generate electron-hole pairs (Eq.4). These pairs interact with water (Eq.5) and dissolved dioxygen (Eq.6), leading to the formation of the •OH and O^{2}•−, respectively[60]. When exposed to a full-spectrum xenon lamp, electrons can swiftly move from the inner to the outer region to engage in surface reactions, resulting in the formation of radicals such as •OH and O^{2}•−. These radicals are extended and stimulated by the more stable •OH radical originating from SiC, which enhances the visible light activity[61]. As a result, a smaller particle size, increased porosity, and surface roughness of the synthesized SiC photocatalyst can contribute to a larger surface area. This can enhance the adsorption of organic compounds and thus, boost the photodegradation rate[62]. The hydroxyl radical, superoxide radical, and vacancy defects of etched nano SiC can degrade organic pollutants[63]. In the EPR diagram, the peak of

superoxide radical by etched nano silicon carbide appears ten minutes after the light is turned on. Conversely, there is no peak in the dark, which indicates that light is helpful in stimulating the generation of superoxide radical on the silicon carbide surface. The vacancy defects were also further enhanced under 10 minutes of illumination, demonstrating that in the whole process of the degradation system, illumination aids the hydroxyl radical, superoxide radical and vacancy defects in degrading dye pollutants, environmental hormones, and medical wastewater[64].

4 Conclusions

In conclusion, we successfully etched silicon carbide in the alkali solution at 90 ℃ and normal pressure, then obtained etched micro silicon carbide, nano silicon carbide, and silicon carbide quantum dots. It was firstly found that alkali etching can dissolve 3-C crystal form faster while retaining 6-H crystal form, which is consistent with the previous report: SiC has high stability in acidic conditions[65]. It could be logically explained by means of cracking of SiC microparticles via the crystallites borders where mixed polytypes are concentrated, followed by selective etching of less stable and polytypes. In addition, the degradation of a wide range of organic pollutants has been successfully achieved on the surface of this material. The concentration of vacancy defects in the etched nano SiC was three orders of magnitude higher than the original sample. The degradation property of the etched nano SiC was 10 times greater than the original sample. In terms of application, the photodegradation process in different acid-base systems and in the presence of 50 μL hydrogen peroxide was analyzed. The concentration of various free radicals was calculated quantitatively by EPR, while the mechanism of photodegradation under the synergistic action of various free radicals was proposed. A highly active and stable catalyst was constructed under full spectrum.

In summary, this study successfully prepared silicon carbide materials with abundant vacancy defects by alkali etching and achieved photodegradation of multiple organic pollutants, bringing new innovations to environmental protection and catalytic applications. Future studies can continue to deepen these findings and promote practical applications of the material in areas such as environmental purification (especially for

various organic pollutants), catalyst development (building high-activity and stable full-spectrum catalysts), material engineering (regulating vacancy defects and surface structure), biomedical applications (eco-friendliness and biocompatibility), and energy fields[66-68]. This novel directional etching enables precise interface control in different polytypes of silicon carbide, opening up a new avenue for improving the purity of single-crystal silicon carbide.

Conflict of Interest

The authors have no conflicts of interest to declare.

Acknowledgement

This work was supported by National Natural Science Foundation (12205056), Natural Science Foundation of Guangxi Province (2021GXNSFBA076003), Guangxi Key Laboratory of Manufacturing Systems and Advanced Manufacturing Technology (20-065-40S007), the Interdisciplinary Scientific Research Foundation of Guangxi University (Grant No. 2022JCA002).

References

1. Besmann, T. M.; Sheldon, B. W.; Lowden, R. A.; Stinton, D. P., Vapor-phase fabrication and properties of continuous-filament ceramic composites. *Science (New York, N.Y.)* **1991,** *253* (5024), 1104-9.
2. Kim, P.; Lieber, C. M., Nanotube nanotweezers. *Science* **1999,** *286* (5447), 2148-2150.
3. Zhang, Y.; Suenaga, K.; Colliex, C.; Iijima, S., Coaxial nanocable: Silicon carbide and silicon oxide sheathed with boron nitride and carbon. *Science* **1998,** *281* (5379), 973-975.
4. Fan, X. J.; Peng, Z. W.; Wang, J. J.; Ye, R. Q.; Zhou, H. Q.; Guo, X., Carbon-Based Composite as an Efficient and Stable Metal-Free Electrocatalyst. *Advanced Functional Materials* **2016,** *26* (21), 3621-3629.
5. Ishikawa, T.; Kohtoku, Y.; Kumagawa, K.; Yamamura, T.; Nagasawa, T., High-strength alkali-resistant sintered SiC fibre stable to 2,200 degrees C. *Nature* **1998,** *391* (6669), 773-775.
6. Bermudez, V. M., Surface science - A metallic semiconductor surface. *Nature Materials* **2003,** *2* (4), 218-219.

7. Daulton, T. L.; Bernatowicz, T. J.; Lewis, R. S.; Messenger, S.; Stadermann, F. J.; Amari, S., Polytype distribution in circumsteller silicon carbide. *Science* **2002,** *296* (5574), 1852-1855.
8. Castelletto, S.; Johnson, B. C.; Ivady, V.; Stavrias, N.; Umeda, T.; Gali, A.; Ohshima, T., A silicon carbide room-temperature single-photon source. *Nature Materials* **2014,** *13* (2), 151-156.
9. Widmann, M.; Lee, S. Y.; Rendler, T.; Son, N. T.; Fedder, H.; Paik, S.; Yang, L. P.; Zhao, N.; Yang, S.; Booker, I.; Denisenko, A.; Jamali, M.; Momenzadeh, S. A.; Gerhardt, I.; Ohshima, T.; Gali, A.; Janzen, E.; Wrachtrup, J., Coherent control of single spins in silicon carbide at room temperature. *Nature Materials* **2015,** *14* (2), 164-168.
10. Christle, D. J.; Falk, A. L.; Andrich, P.; Klimov, P. V.; Ul Hassan, J.; Son, N. T.; Janzen, E.; Ohshima, T.; Awschalom, D. D., Isolated electron spins in silicon carbide with millisecond coherence times. *Nature Materials* **2015,** *14* (2), 160-163.
11. Peng, Y.; Wang, L.; Luo, Q.; Cao, Y.; Dai, Y.; Li, Z.; Li, H.; Zheng, X.; Yan, W.; Yang, J.; Zeng, J., Molecular-Level Insight into How Hydroxyl Groups Boost Catalytic Activity in CO2 Hydrogenation into Methanol. *Chem* **2018,** *4* (3), 613-625.
12. Li, Y.; Liu, X.; Liang, T.; Fan, J., Core and Surface Electronic States and Phonon Modes in SiC Quantum Dots Studied by Optical Spectroscopy and Hybrid TDDFT. *The Journal of Physical Chemistry C* **2021,** *125* (13), 7259-7266.
13. Zhu, J.; Hu, S.; Xia, W.-w.; Li, T.-h.; Fan, L.; Chen, H.-t., Photoluminescence of ~2nm 3C–SiC quantum dots fabricated from polycrystalline 6H–SiC target by pulsed laser ablation. *Materials Letters* **2014,** *132*, 210-213.
14. Fan, J.; Li, H.; Wang, J.; Xiao, M., Fabrication and photoluminescence of SiC quantum dots stemming from 3C, 6H, and 4H polytypes of bulk SiC. *Applied Physics Letters* **2012,** *101* (13).
15. Li, X. X.; Li, W. J.; Liu, Q.; Chen, S. L.; Wang, L.; Gao, F. M.; Shao, G.; Tian, Y.; Lin, Z. F.; Yang, W. Y., Robust High-Temperature Supercapacitors Based on SiC Nanowires. *Advanced Functional Materials* **2021,** *31* (8).
16. An, Z.; Ye, C.; Zhang, R.; Zhou, P., Flexible and recoverable SiC nanofiber aerogels for electromagnetic wave absorption. *Ceramics International* **2019,** *45* (17), 22793-22801.
17. Li, B.; Song, Y.-C.; Zhang, C.-R.; Yu, J.-S., Synthesis and characterization of nanostructured silicon carbide crystal whiskers by sol–gel process and carbothermal reduction. *Ceramics International* **2014,** *40* (8), 12613-12616.
18. Shi, Y. F.; Zhang, F.; Hu, Y. S.; Sun, X. H.; Zhang, Y. C.; Lee, H. I.; Chen, L. Q.; Stucky, G. D., Low-Temperature Pseudomorphic Transformation of Ordered Hierarchical Macro-mesoporous SiO2/C Nanocomposite to SiC via Magnesiothermic Reduction. *Journal of the American Chemical Society* **2010,** *132* (16), 5552-+.
19. Luo, F.; Jiang, R.; Hu, X.; He, Z.; Wang, Y., Structure and properties of nano SiC coatings in-situ fabricated by laser irradiation. *Ceramics International* **2020,** *46* (10), 14747-14755.
20. Luo, T.; Chen, X.; Wang, L.; Wang, P.; Li, C.; Iqbal, S.; Cao, B., Ultrafast synthesis of SiC@graphene nanocomposites by one-step laser induced fragmentation and decomposition. *Ceramics International* **2018,** *44* (15), 19028-19032.

21. Xue, J.; Yin, X.; Ye, F.; Zhang, L.; Cheng, L.; Bessman, T., Thermodynamic Analysis on the Codeposition of SiC-Si3N4 Composite Ceramics by Chemical Vapor Deposition using SiCl4-NH3-CH4-H2-Ar Mixture Gases. *Journal of the American Ceramic Society* **2013,** *96* (3), 979-986.
22. Michaels, J. A.; Janavicius, L.; Wu, X.; Chan, C.; Huang, H. C.; Namiki, S.; Kim, M.; Sievers, D.; Li, X., Producing Silicon Carbide Micro and Nanostructures by Plasma-Free Metal-Assisted Chemical Etching. *Advanced Functional Materials* **2021,** *31* (32).
23. Cambaz, G. Z.; Yushin, G. N.; Gogotsi, Y.; Lutsenko, V. G., Anisotropic etching of SiC whiskers. *Nano Letters* **2006,** *6* (3), 548-551.
24. Zhan, S.; Dong, B.; Wang, H.; Zhao, Y., A novel approach for bulk micromachining of 4H-SiC by tool-based electrolytic plasma etching in HF-free aqueous solution. *Journal of the European Ceramic Society* **2021,** *41* (10), 5075-5087.
25. Khuat, V.; Ma, Y.; Si, J.; Chen, T.; Chen, F.; Hou, X., Fabrication of through holes in silicon carbide using femtosecond laser irradiation and acid etching. *Applied Surface Science* **2014,** *289*, 529-532.
26. Michaels, J. A.; Janavicius, L.; Wu, X. H.; Chan, C.; Huang, H. C.; Namiki, S.; Kim, M.; Sievers, D.; Li, X. L., Producing Silicon Carbide Micro and Nanostructures by Plasma-Free Metal-Assisted Chemical Etching. *Advanced Functional Materials* **2021,** *31* (32).
27. Zhang, Y.; Chen, H.; Liu, D.; Deng, H., High efficient polishing of sliced 4H-SiC (0001) by molten KOH etching. *Applied Surface Science* **2020,** *525*.
28. Shi, M. J.; Wang, R. Y.; Li, L. Y.; Chen, N. T.; Xiao, P.; Yan, C.; Yan, X. B., Redox-Active Polymer Integrated with MXene for Ultra-Stable and Fast Aqueous Proton Storage. *Advanced Functional Materials*.
29. Kato, M.; Watanabe, O.; Mii, T.; Sakane, H.; Harada, S., Suppression of stacking-fault expansion in 4H-SiC PiN diodes using proton implantation to solve bipolar degradation. *Sci Rep* **2022,** *12* (1), 18790.
30. Wang, M. F.; Liu, S. S.; Ji, H. Q.; Liu, J.; Yan, C. L.; Qian, T., Unveiling the Essential Nature of Lewis Basicity in Thermodynamically and Dynamically Promoted Nitrogen Fixation. *Advanced Functional Materials* **2020,** *30* (32).
31. Song, N.; Liu, H.; Yuan, Y. T.; Li, X.; Fang, J. Z., Fabrication and Corrosion Resistance of SiC-coated Multi-walled Carbon Nanotubes. *Journal of Materials Science & Technology* **2013,** *29* (12), 1146-1150.
32. Wang, W.; Jin, Z.; Xue, T.; Yang, G.; Qiao, G., Preparation and characterization of SiC nanowires and nanoparticles from filter paper by sol–gel and carbothermal reduction processing. *Journal of Materials Science* **2007,** *42* (15), 6439-6445.
33. Treffer, G.; Neuhauser, J.; Marx, G., XRD-studies of SiC/Si layers on carbon substrates. *Mikrochimica Acta* **1997,** *125* (1-4), 325-330.
34. Rufangura, P.; Khodasevych, I.; Agrawal, A.; Bosi, M.; Folland, T. G.; Caldwell, J. D.; Iacopi, F., Enhanced Absorption with Graphene-Coated Silicon Carbide Nanowires for Mid-Infrared Nanophotonics. *Nanomaterials* **2021,** *11* (9).

35. Koysuren, O., Improving ultraviolet light photocatalytic activity of polyaniline/silicon carbide composites by Fe-doping. *Journal of Applied Polymer Science* **2019,** *137* (14).
36. Ahmed, Y. M. Z.; El-Sheikh, S. M., Influence of the pH on the Morphology of Sol-Gel-Derived Nanostructured SiC. *Journal of the American Ceramic Society* **2009,** *92* (11), 2724-2730.
37. Qin, X.; Li, X.; Chen, X.; Yang, X.; Zhang, F.; Xu, X.; Hu, X.; Peng, Y.; Yu, P., Raman scattering study on phonon anisotropic properties of SiC. *Journal of Alloys and Compounds* **2019,** *776*, 1048-1055.
38. Chang, Y.; Xiao, A. X.; Li, R. B.; Wang, M. J.; He, S. S.; Sun, M. Y.; Wang, L. Z.; Qu, C. Y.; Qiu, W., Angle-Resolved Intensity of Polarized Micro-Raman Spectroscopy for 4H-SiC. *Crystals* **2021,** *11* (6).
39. Ohmukai, M.; Naito, H.; Okuda, M.; Kurosawa, K., Characteristics of amorphous silicon precipitated by means of argon excimer laser irradiation on SiC films. *Journal of Non-Crystalline Solids* **1996,** *202* (1-2), 77-80.
40. Li, X.; Wei, J.; Chen, B.; Wang, Y.; Jiang, C.; Zhang, H.; Qiao, M., Effective electromagnetic wave absorption and photoluminescence performances of flexible SiC nanowires membrane. *Ceramics International* **2021,** *47* (12), 17615-17626.
41. Fu, X.; Wang, D., Effect of stacking fault nanolayers on the photoluminescence properties of SiC nanowires. *Applied Surface Science* **2019,** *493*, 497-505.
42. Tran, T. T.; Bray, K.; Ford, M. J.; Toth, M.; Aharonovich, I., Quantum emission from hexagonal boron nitride monolayers. *Nature Nanotechnology* **2016,** *11* (1), 37-+.
43. Han, M. K.; Yin, X. W.; Hou, Z. X.; Song, C. Q.; Li, X. L.; Zhang, L. T.; Cheng, L. F., Flexible and Thermostable Graphene/SiC Nanowire Foam Composites with Tunable Electromagnetic Wave Absorption Properties. *Acs Applied Materials & Interfaces* **2017,** *9* (13), 11803-11810.
44. Wei, J.; Li, X.; Wang, Y.; Chen, B.; Zhang, M.; Qin, C., Photoluminescence property of inexpensive flexible SiC nanowires membrane by electrospinning and carbothermal reduction. *Journal of the American Ceramic Society* **2020,** *103* (11), 6187-6197.
45. Wang, H. Y.; Jiang, W. F.; Kang, L. P.; Li, Z. J., Photoluminescence and electron field-emission properties of SiC-SiO2 core-shell fibers and 3C-SiC nanowires on silicon nanoporous pillar array. *Journal of Alloys and Compounds* **2013,** *553*, 125-128.
46. Shen, Z.; Chen, J.; Li, B.; Li, G.; Zheng, H.; Men, J.; Hou, X., Tunable fabrication and photoluminescence property of SiC nanowires with different microstructures. *Applied Surface Science* **2020,** *506*.
47. Yang, S. K.; Cai, W. P.; Zeng, H. B.; Xu, X. X., Ultra-fine beta-SiC quantum dots fabricated by laser ablation in reactive liquid at room temperature and their violet emission. *Journal of Materials Chemistry* **2009,** *19* (38), 7119-7123.
48. Guo, Z.; Qiu, S.; Li, H.; Xu, Y.; Langford, S. J.; Sun, C., Electrocatalytic dinitrogen reduction reaction on silicon carbide: a density functional theory study. *Phys Chem Chem Phys* **2020,** *22* (38), 21761-21767.
49. Yang, J.; Feng, J. X.; Li, W. Q.; Chen, X. X.; Liu, X. S.; Ruan, J. J.; Qiu, R. L.; Xiong, Y.; Tian, S. H., A resource-utilization way of the waste printed circuit boards to

prepare silicon carbide nanoparticles and their photocatalytic application. *Journal of Hazardous Materials* **2019,** *373*, 640-648.
50. Lewandkow, R.; Mazur, P.; Trembulowicz, A.; Sabik, A.; Wasielewski, R.; Grodzicki, M., Influence of Graphite Layer on Electronic Properties of MgO/6H-SiC(0001) Interface. *Materials (Basel)* **2021,** *14* (15).
51. Maruyama, T.; Bang, H.; Fujita, N.; Kawamura, Y.; Naritsuka, S.; Kusunoki, M., STM and XPS studies of early stages of carbon nanotube growth by surface decomposition of 6H–SiC(000-1) under various oxygen pressures. *Diamond and Related Materials* **2007,** *16* (4-7), 1078-1081.
52. Yagyu, K.; Takahashi, K.; Tochihara, H.; Tomokage, H.; Suzuki, T., Neutralization of an epitaxial graphene grown on a SiC(0001) by means of palladium intercalation. *Applied Physics Letters* **2017,** *110* (13).
53. Hasegawa, M.; Sugawara, K.; Suto, R.; Sambonsuge, S.; Teraoka, Y.; Yoshigoe, A.; Filimonov, S.; Fukidome, H.; Suemitsu, M., In Situ SR-XPS Observation of Ni-Assisted Low-Temperature Formation of Epitaxial Graphene on 3C-SiC/Si. *Nanoscale Res Lett* **2015,** *10* (1), 421.
54. Liu, X.; Cheng, L.; Zhang, L.; Yin, X.; Dong, N.; Zhao, D.; Hong, Z.; Li, Z., Erosion Behavior of C/SiC Composites in Atomic Oxygen. *International Journal of Applied Ceramic Technology* **2013,** *10* (1), 168-174.
55. Shimoda, K.; Park, J.-S.; Hinoki, T.; Kohyama, A., Influence of surface structure of SiC nano-sized powder analyzed by X-ray photoelectron spectroscopy on basic powder characteristics. *Applied Surface Science* **2007,** *253* (24), 9450-9456.
56. Wang, B.; Yin, J.; Chen, D.; Long, X.; Li, L.; Lin, H.-H.; Hu, W.; Talwar, D. N.; Jia, R.-X.; Zhang, Y.-M.; Ferguson, I. T.; Sun, W.; Feng, Z. C.; Wan, L., Optical and surface properties of 3C–SiC thin epitaxial films grown at different temperatures on 4H–SiC substrates. *Superlattices and Microstructures* **2021,** *156*.
57. Miao, K. C.; Bourassa, A.; Anderson, C. P.; Whiteley, S. J.; Crook, A. L.; Bayliss, S. L.; Wolfowicz, G.; Thiering, G.; Udvarhelyi, P.; Ivady, V.; Abe, H.; Ohshima, T.; Gali, A.; Awschalom, D. D., Electrically driven optical interferometry with spins in silicon carbide. *Science Advances* **2019,** *5* (11).
58. Christle, D. J.; Klimov, P. V.; de las Casas, C. F.; Szász, K.; Ivády, V.; Jokubavicius, V.; Ul Hassan, J.; Syväjärvi, M.; Koehl, W. F.; Ohshima, T.; Son, N. T.; Janzén, E.; Gali, Á.; Awschalom, D. D., Isolated Spin Qubits in SiC with a High-Fidelity Infrared Spin-to-Photon Interface. *Physical Review X* **2017,** *7* (2).
59. Kondo, S.; Seki, K.; Maeda, Y.; Yu, H.; Fukami, K.; Kasada, R., Contribution of dangling-bonds to polycrystalline SiC corrosion. *Scripta Materialia* **2020,** *188*, 6-9.
60. Marien, C. B. D.; Le Pivert, M.; Azais, A.; M'Bra, I. C.; Drogui, P.; Dirany, A.; Robert, D., Kinetics and mechanism of Paraquat's degradation: UV-C photolysis vs UV-C photocatalysis with TiO2/SiC foams. *Journal of Hazardous Materials* **2019,** *370*, 164-171.
61. G, M.; A, S.; G.A, S. J.; S, K., Preparation, characterization and enhanced photocatalytic activities of zinc oxide nano rods/silicon carbide composite under UV and visible light irradiations. *Journal of Molecular Catalysis A: Chemical* **2016,** *411*, 167-178.

62. Dang, H.; Li, B.; Li, C.; Zang, Y.; Xu, P.; Zhao, X.; Fan, H.; Qiu, Y., One-dimensional Au/SiC heterojunction nanocomposites with enhanced photocatalytic and photoelectrochemical performances: Kinetics and mechanism insights. *Electrochimica Acta* **2018,** *267*, 24-33.
63. Qian, S.; Qiao, F.; Zhou, L.; Liu, Y.; Liu, W.; Yang, J.; Wang, T.; Li, H., Performance and mechanism analysis of photocatalytic degradation of tetracycline by SiC/CdS composites. *CrystEngComm* **2022,** *24* (35), 6269-6277.
64. Zhang, Y.; Zhang, Y.; Li, X.; Dai, J.; Song, F.; Cao, X.; Lyu, X.; Crittenden, J. C., Enhanced Photocatalytic Activity of SiC-Based Ternary Graphene Materials: A DFT Study and the Photocatalytic Mechanism. *ACS Omega* **2019,** *4* (23), 20142-20151.
65. Kato, M.; Watanabe, O.; Mii, T.; Sakane, H.; Harada, S. Suppression of stacking-fault expansion in 4H-SiC PiN diodes using proton implantation to solve bipolar degradation. *Scientific Reports* **2022**, 12 (1). 2045-2322.
66. Botsoa, J.; Lysenko, V.; Geloen, A.; Marty, O.; Bluet, J. M.; Guillot, G. Application of 3C-SiC quantum dots for living cell imaging. *Applied Physics Letters* **2008**, 92 (17). 0003-6951
67. Amato, M.; Rurali, R. Shell-Thickness Controlled Semiconductor-Metal Transition in Si-SiC Core-Shell Nanowires. *Nano Letters* **2015**, 15 (5), 1530-6984.
68. Zhu, Z. Q.; Yang, L. L.; Xiong, Z. D.; Liu, D. H.; Hu, B. B.; Wang, N. N.; Ola, O.; Zhu, Y. Q. SiC@FeZnZiF as a Bifunctional Catalyst with Catalytic Activating PMS and Photoreducing Carbon Dioxide. Nanomaterials 2023, 13 (10).

Declaration of interests

☒ The authors declare that they have no known competing financial interests or personal relationships that could have appeared to influence the work reported in this paper.

☐ The authors declare the following financial interests/personal relationships which may be considered as potential competing interests: